Environ. Sci. Technol. **1998**, *32,* 398−404

Mathematical Model of a Photocatalytic Fiber-Optic Cable Reactor for Heterogeneous Photocatalysis

NICOLA J. PEILL AND
MICHAEL R. HOFFMANN*
W. M. Keck Laboratories, California Institute of Technology, Pasadena, California 91125

A basic mathematical model to describe the degradation of a single compound in a fiber-optic bundled array photocatalytic batch reactor (OFR) using a Langmuir−Hinshelwood kinetic expression is developed. An empirical global quantum efficiency, ϕ_{global}, that incorporates reaction parameters such as the absorbed light intensity, intrinsic rate constants, concentration of adsorbed reactants, and reaction intermediates is used as a fitting parameter. An empirical term to describe the radiation field within the coated fiber is derived experimentally and normalized by the photocatalyst particle concentration within the fiber optic coating to account for the inverse relationship observed between absorbed light intensity and reaction quantum efficiency. Results of the mathematical model are compared to experimental data generated in an OFR for the photocatalytic oxidation of 4-chlorophenol (4CP), pentachlorophenol (PCP), and dichloroacetate (DCA). The global quantum efficiency, ϕ_{global}, was found to be independent of absorbed light intensity. Calculated kinetic profiles are in excellent agreement with experimental observation.

Introduction

Fixed-bed photocatalytic optical fiber reactor systems (OFR) for the remediation of polluted waste streams (*1*−*4*) may provide a practical alternative to conventional photochemical reactor systems. The fiber-optic cable is used both for remote light transmission and for the solid support of the photocatalyst. This reactor configuration has several advantages over slurry-phase and conventional fixed-bed reactor designs (*5*). Direct delivery of light to the photocatalyst minimizes losses due to absorption and scattering by the reactor and reaction solution. The dispersed coated fiber configuration provides a more uniform distribution of the photocatalyst within the reaction solution resulting in reduced mass transport limitations to photochemical conversion and allowing for higher processing capacities (*1*). Distribution of the input light intensity over a large number of coated fibers minimizes the incident light intensity to which the photocatalyst is exposed. This effect has been shown to enhance the relative quantum efficiency to photochemical conversion (*5*−*12*). Futhermore, the remote transmission of light to a photocatalyst via a fiber-optic cable system is not possible with other photocatalytic reactor configurations. As a result, an OFR system could be utilized for *in situ* remediation of contaminated subsurface environments and for the remote, offline treatment of either aqueous- and/or vapor-phase contaminants such as chlorinated hydrocarbons.

The use of optical fibers as a means of light transmission and distribution to solid-supported photocatalysts was first proposed by Ollis and Marinangeli (*13*−*15*). However, their theoretical analysis, which assumed an strict evancescent wave mechanism for light propagation, concluded that photocatalytic−optical fiber reactor systems would not be practical due to catalyst deactivation caused by heat buildup in a bundled fiber array. In a later study, Gapen and Anderson (*16*) tested an optical fiber reactor, but they encountered problems with delamination of the TiO_2 coating and, as a consequence, observed only a partial photodegradation of 3-chlorosalicylic acid. They concluded that a method for obtaining a stable photocatalytic coating needed to be developed before an optical fiber system would be practical. In order to address some of these problems, we constructed and characterized several different fixed-bed photocatalytic reactor systems that employ fiber-optic cables (*1*−*4*). These systems were designed for the remote delivery of light to the photocatalyst, to allow for measurement of light fluxes for direct determination of quantum yields and for reuse of the reactor to test various coatings and light input angles, and to minimize possible heat buildup and delamination problems.

In order to better understand the OFR system illustrated in Figure 1, we now present a mathematical model to describe the degradation of a single compound in an OFR using a Langmuir−Hinshelwood kinetic expression. We assume that the reaction is not mass-transport limited and that the overall process can be represented by a single coated fiber immersed in a differential reaction volume, as shown in Figure 2, and that the reaction occurs exclusively at the solution/coating interface (*1*). The radiation field in a coated fiber is unique from slurry-phase and other fixed-bed reactor configurations. As light travels down a coated fiber, it is refracted out of the fiber and directly into the semiconductor coating and undergoes an exponential decay in illumination intensity downward along the length of the fiber. If the coating layer is of sufficient thickness and the coated fiber is of sufficient length, then all of the input light is absorbed by the coating over the length of the fiber. A term describing the absorbed light intensity as a function of position in the fiber, $I'_{abs}(z)$, and Langmuir−Hinshelwood constants (*17*) are derived experimentally. The global quantum efficiency, ϕ_{global}, which is modeled as a function of the absorbed light intensity, is used as a fitting parameter. The model is tested against experimental data generated in an OFR for the photocatalytic oxidation of 4-chlorophenol (4CP), pentachlorophenol (PCP), and dichloroacetate (DCA) (*3*), and model values for ϕ_{global} are compared to experimental values.

Experimental Section

OFR Oxidations. The basic features of the OFR system, which is illustrated in Figure 1, have been described in detail elsewhere (*2*). The key components are a xenon-arc UV radiation source, a 310−375-nm band pass filter, a focusing lens, a light transmitting TiO_2-coated fiber-optic bundle consisting of 72 1-mm diameter, 1.2 m long fibers (3M PowerCore FT-1.0-UMT), and a 227-mL cylindrical Pyrex reaction vessel with a bottom-fritted gas inlet. The TiO_2-laden fibers were prepared by stripping the terminal 20 cm of the fibers to expose the quartz core, coating with a 13 wt % aqueous

* To whom correspondence should be addressed. E-mail: mrh@cco.caltech.edu; Fax: 626-395-3170.

S0013-936X(96)00874-7 CCC: $15.00
Published on Web 01/01/1998

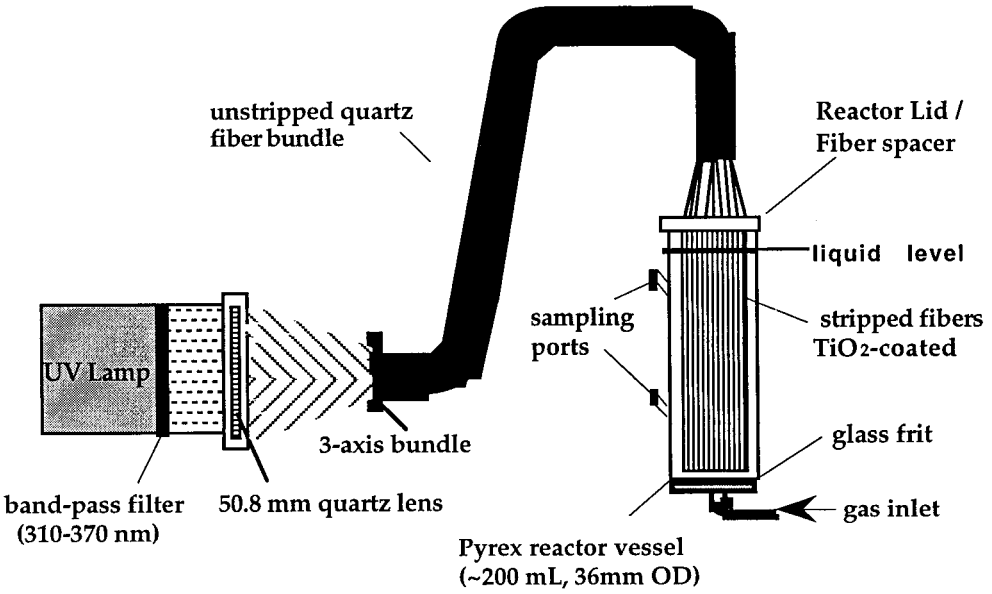

FIGURE 1. Schematic of optical-fiber bundled array photocatalytic reactor system.

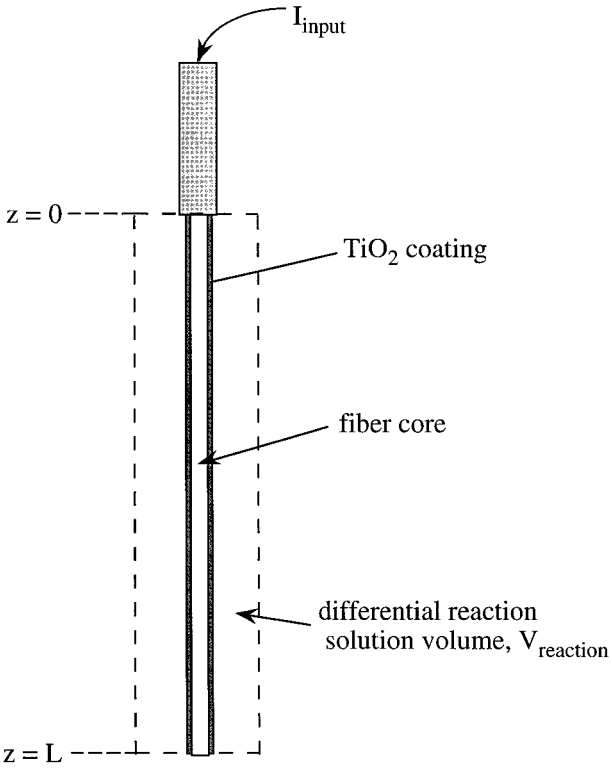

FIGURE 2. Model scheme: a single, coated optical fiber with length *L* immersed in a differential reaction solution volume, $V = V_{reactor}$/ number of fibers.

slurry of TiO_2 (Degussa P25), and annealing at 300 °C maximum.

Input and absorbed light intensities for the single fiber light distribution and OFR oxidation experiments were measured by chemical actinometry using α-(2,5-dimethyl-3-furylethylidene) (isopropylidene) succinic anhydride (Aberchrome 540). The experimental methods and results have been previously described (*2*). Light flux measurements were made for uncoated and coated fibers. The difference between the two was taken to be the total photon flux absorbed by the TiO_2 layer, $I_{abs(bundle)}$. The light intensities into individual fibers, I_{input}, were estimated by dividing $I_{abs(bundle)}$ by the total number of coated fibers in the bundle.

TABLE 1. Slurry-Phase Reaction Conditions and Measured Rate Constants, k_{slurry}, and Absorption Equilibrium Constants, K_{ads}, for 4CP, PCP, and DCA[a]

compd	$[C]_o$ (mM)/$pH_{initial}$ − pH_{final}	k_{slurry} (μmol (min·$g_{catalyst}$)$^{-1}$)	K_{ads} (μM^{-1})
4CP	0.20, 0.10, 0.060, 0.030/5.5	1.30	0.020
PCP	0.061, 0.040, 0.030, 0.020/ 4.5−5.5	2.5	0.017
DCA	2.0, 1.0, 0.3/3.0	10.8	0.0027

[a] $[TiO_2] = 0.5$ g L^{-1}, $I_{input} = 50$ μE L^{-1} min^{-1}.

Sample solutions (190 mL) of reagent-grade 4CP (Aldrich), PCP (Aldrich), and DCA (Spectrum) of varying initial concentrations and pH (Table 1) were prepared from stock solutions. Before irradiation, the coated-fiber bundle was immersed in the reaction solution and allowed to equilibrate for 30 min. Nylon (Nalgene 0.45 μm) or Teflon (Acrodisc 4CRPTFE 0.45 μm) syringe filters were used to filter all samples. Pure oxygen (Air Liquide) was used at saturation in water as the primary electron acceptor. The reactor was mixed via continuous sparging with O_2.

An equivalent slurry-phase TiO_2 loading (ESPL) of 0.5 g L^{-1} was determined by stripping 13 wt % TiO_2 coatings from the fibers by immersing the fibers in distilled water at pH 11 (KOH) and sonicating overnight. The TiO_2 sludge was recovered, dried, and weighed. Several measurements were made and averaged. The ESPL is calculated as the mass of recovered catalyst divided by the reaction solution volume (0.19 L). This value is representative of the ESPL of the single fiber reaction scheme shown in Figure 2.

Slurry-Phase Oxidations. Vigorously stirred, air-saturated sample solutions (30 mL) of 4CP, PCP, and DCA of varying initial concentrations (Table 1) and containing 0.5 g L^{-1} TiO_2 (Degussa P25) were irradiated for 1 h. The light intensity was adjusted using a neutral density filter to achieve an input light intensity similar to that of the OFR (50 μE L^{-1} min^{-1}).

Sample Analysis. 4CP and PCP were analyzed by HPLC using a Hewlett Packard ODS Hypersil (5 μm) column with an eluent (1 mL min^{-1}) of 20/80% acetonitrile/water (pH 3) and 65/35% methanol/water, respectively. DCA was quantified by ion chromatography (Dionex BIOLC 4500i series) using an Ionpac AG11 Guard column with an eluent (1 mL min^{-1}) of 75/25% 5 mM/100 mM NaOH. The pH was determined

with a Radiometer PHM85 pH meter. A constant pH was maintained for the PCP and DCA oxidations by the addition of KOH (Mallinckrodt AR) (Table 1).

Model Development

A rate expression for a single-component heterogeneous photocatalytic batch reaction may be described by a saturation kinetic expression as follows (*18*):

$$-\frac{dC_R(t)}{dt} = \frac{\hat{s}\omega}{V} k_{obs} \frac{K_{ads} C_R(t)}{1 + K_{ads} C_R(t)} \quad (1)$$

where $\hat{s}$ is the moles of surface sites per mass of catalyst (μmol $g_{catalyst}^{-1}$), ω is the photocatalyst loading on the fiber (g), V is the differential reaction volume around the coated fiber (L), k_{obs} is an observed rate constant (min^{-1}), K_{ads} is the dynamic Langmuir adsorption constant (μM^{-1}), and $C_R(t)$ is the time-dependent concentration of reactant R (μM). Application of eq 1 assumes that (a) the reaction is surface mediated and (b) the reaction system is in dynamic equilibrium and driven by reaction kinetics and not adsorption kinetics. Furthermore, it is assumed that competition for surface sites by intermediates and other solution-phase species such as O_2 are not rate limiting.

If the above assumptions are valid, then the basic elements in the reaction system include the reactants (e.g., R, O_2, etc.), the adsorption surface sites, and the photocatalytically-generated oxidants, $^{\bullet}OH_{ads}$ and h_{vb}^{+}, and primary reduced dioxygen species, $O_2^{\bullet -}$. The first term in eq 1 quantifies the concentration of adsorption surface sites available while the Langmuir saturation term ($K_{ads}C_R(t)$)/[1 + K_{ads}CR(t)] represents the fraction of surface sites occupied by R. Together these terms quantify the surface concentration of the reactant R. The observed rate constant, k_{obs}, then contains the remaining reaction parameters, which may include the intrinsic reaction rate constant, the rate of $OH^{\bullet}$ and $O_2^{\bullet -}$ generation, a function of the absorbed photon flux, I_{abs}, $[O_2]_{ads}$, competition from intermediate species, and mass transport effects (*7*, *18*−*20*).

The dependency of reaction rate and quantum efficiency on the absorbed light intensity has been well established (*3*, *5*−*12*, *21*), where the experimental quantum efficiency (i.e., relative quantum efficiency) is defined as

$$\phi_{exp} = \frac{\left|\frac{-d[4CP]}{dt}\right|}{\left|\frac{d[h\nu]_{abs}}{dt}\right|} \cong \frac{\text{initial reaction rate}}{\text{absorbed light flux}} \quad (2)$$

where $d[h\nu]_{abs}/dt \equiv I_{abs}$. In general, the observed photochemcial reaction rates vary linearly with I_{abs} at absorbed light intensities significantly below one sun (~60 W m^{-2}), vary as the square root of I_{abs} at moderate illumination intensities, and is independent of I_{abs} at higher light fluxes (i.e., the relative quantum efficiency varies either as I_{abs}^{0}, $I_{abs}^{-0.5}$, or I_{abs}^{-1} depending on the magnitude of I_{abs}).

A global reaction quantum efficiency, ϕ_{global}, is expressed as follows:

$$\phi_{global} = f(I_{abs}, k_{intrinsic}, [O_2]_{ads}, \sum_{i}^{n} C_{i,ads}) \quad (3)$$

where

$$k_{obs} = \hat{I}_{abs}\, \phi_{global} \quad (4)$$

and $\hat{I}_{abs}$ is the light intensity absorbed by the photocatalytic coating normalized by the coating'' photocatalytic particle density, $\hat{\omega}$, given by

$$\hat{\omega} = \frac{\omega}{V_{coating}} (MW_{TiO_2}\gamma)^{-1} \quad (5)$$

where γ is the number of TiO_2 molecules per TiO_2 particle with an estimated value of 4.16×10^5 for Degussa P25 (*22*), and MW_{TiO_2} is the molecular weight of TiO_2.

In a coated fiber, the absorbed light intensity varies along the length of the fiber, z, and, as a consequence, $\phi_{global}(I_{abs})$ also varies with z. We express the absorbed light intensity as a function of fiber length and integrate the product over the length of the coated fiber:

$$k_{obs} = \hat{\omega}^{-1} \int_0^l \{I'_{abs}(z)\phi_{global}(I'_{abs}(z))\}\, dz \quad (6)$$

where $I'_{abs}(z)$ has units of $\mu E\, L^{-1}\, min^{-1}\, m^{-1}$ and $\hat{\omega}$ is assumed to be constant over the entire length of the fiber, l.

Refraction of light out of an optical fiber and into a photocatalytic coating is the primary loss mechanism as light is transmitted down the fiber (*2*). Experimental data suggest that the refractive loss can be represented by an exponential decay of the form (vide infra):

$$I_{fiber}(z) = I_{input} e^{-\alpha z} \quad (7)$$

where $I_{fiber}(z)$ is the amount of light remaining in the fiber at position z ($\mu E\, L^{-1}\, min^{-1}$); I_{input} is the light in the fiber at position $z = 0$; and α is a refractive loss coefficient that is a function of the optical and physical properties of the fiber core and the photocatalytic coating (m^{-1}). The amount of light refracted out of the fiber and into the coating as a function of position along the fiber is given by

$$I'_{abs}(z) = -\frac{dI_{fiber}(z)}{dz} = \alpha I_{input}\, e^{-\alpha z} \quad (8)$$

The dependence of the relative quantum efficiency on the absorbed light intensity can be fit to a power law expression

$$\phi_{global}(I'_{abs}(z)) = A I'_{abs}(z)^{-\beta} \quad (9)$$

Substituting the expressions for $I'_{abs}(z)$ and $\phi_{global}(I'_{abs}(z)$ into eqs 6 and 1 gives

$$-\frac{dC_R(t)}{dt} = \frac{\hat{s}\omega}{V}\frac{A}{\hat{\omega}}\alpha^{(1-\beta)} I_{input}^{(1-\beta)} \{\int_0^L e^{-(1-\beta)\alpha z}\, dz\} \frac{K_{ads} C_R(t)}{1 + K_{ads} C_R(t)} \quad (10)$$

Integration of eq 10 with respect to time gives an implicit solution for $C_R(t)$

$$\frac{1}{K_{ads}} \ln (C_R(t)) + C_R(t) = \frac{1}{K_{ads}} \ln (C(0)_R) + C(0)_R' - \chi t \quad (11)$$

where

$$\chi = \frac{\hat{s}\omega A \alpha^{-\beta} I^{(1-\beta)}{}_{input}}{V\hat{\omega}(1-\beta)} \{1 - e^{-(1-\beta)\alpha^L}\} \quad (12)$$

Results

Model Parameter Estimation. Refractive light losses from single-fiber loss experiments for two coating thicknesses, that were obtained from our previously published results on the OFR system (*1*, *2*), were fit to eq 7, as shown in Figure 3. In these cases, α was found to be 20 and 40 m^{-1} for 13 and 17 wt % TiO_2 coatings, respectively. A curve fit of eq 9 to intensity-dependent quantum efficiency data for the photocatalytic oxidation of 4CP in the OFR gives values of 0.025 and 0.3 for A and β, respectively (Figure 4). It should

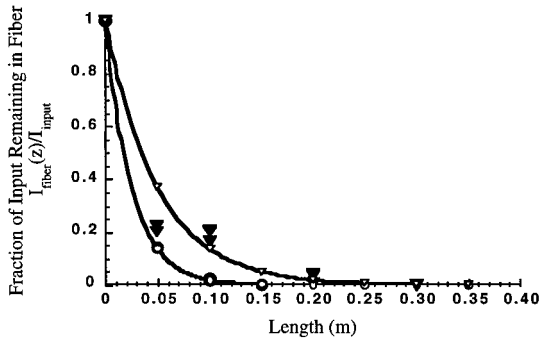

FIGURE 3. Light intensity distribution in a single fiber for a 13 wt % TiO_2 coating (P) experimental data and (S) curve fit: $I_{fiber}(z)/I_{input} = e^{-20*z}$; and 17 wt% TiO_2 coating (J) experimental data and (E) curve fit: $I_{fiber}(z)/I_{input} = e^{-40*z}$.

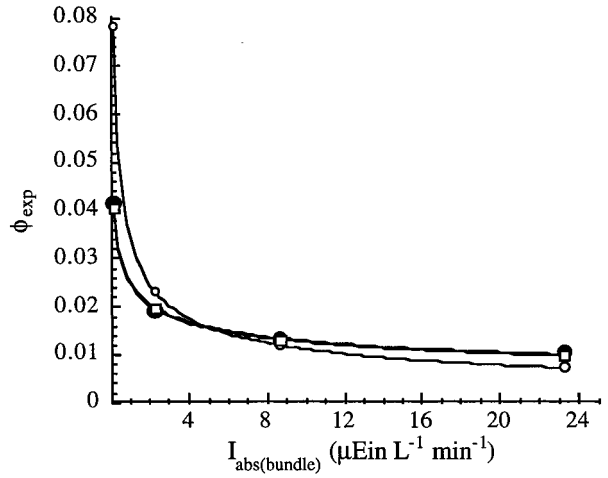

FIGURE 4. Relative quantum efficiency, ϕ_{exp}, as a function of absorbed light intensity for the photocatalytic oxidation of 4CP in OFR; (J) experimental data; (G) $\phi(I_{abs}) = 0.025 I_{abs}^{-0.3}$; and (É) $\phi(I_{abs}) = 0.035 I_{abs}^{-0.5}$ and curve fits. Reaction conditions are given in the text.

be noted that the curve fit was derived using measured values of I_{abs} rather than $I'_{abs}(z)$.

Slurry-phase photocatalytic oxidations of 4CP, PCP, and DCA were carried out at several initial concentrations and under reaction conditions similar to those of the OFR experiments for pH, $[TiO_2]$, and I_{input} to estimate values for the Langmuir adsorption constant, K_{ads}. Values for K_{ads} listed in Table 1 are derived from linear fits of $rate^{-1}$ versus $[R]^{-1}$ where the slope is $(k_{slurry}K_{ads})^{-1}$, the intercept equals $(k_{slurry})^{-1}$, and k_{slurry} is the observed reaction rate constant for the slurry-phase reaction. A sample plot for 4-chlorophenol is shown in Figure 5.

Comparison to Experimental OFR Data. A representative plot comparing experimental data and model calculations for 4CP oxidation is shown in Figure 6. The model is run for three $\phi_{global}(I'_{abs}(z))$ functions: case 1, $\phi_{global} = A$; case 2, $\phi_{global} = A(I'_{abs}(z))^{-0.3}$; and case 3, $\phi_{global} = A(I'_{abs}(z))^{-0.5}$ and $I_{input} = 0.3\,\mu E\,L^{-1}\,min^{-1}$. The absorbed light intensity is normalized by $\hat{\omega}$, which has a value of 4.1 μM (i.e., TiO_2 as particles) as determined by eq 5. The coating thickness, length, and porosity are 5 μm, 0.20 m, and 0.9, respectively, and $\omega/V_{coating} = 0.48$ g L^{-1}. These values are consistent with previous findings (*2*, *3*). $\hat{s}$ is estimated to be 300 μmol sites $g^{-1}_{catalyst}$ based on a reported value of three to four surface sites nm^{-2} (*23*). *A* was varied until a reasonable fit to the data was achieved. Table 2 gives the best-fit values of *A* for each case and the corresponding values of ϕ_{exp} and average ϕ_{global} for the oxidation of 4CP, PCP, and DCA where

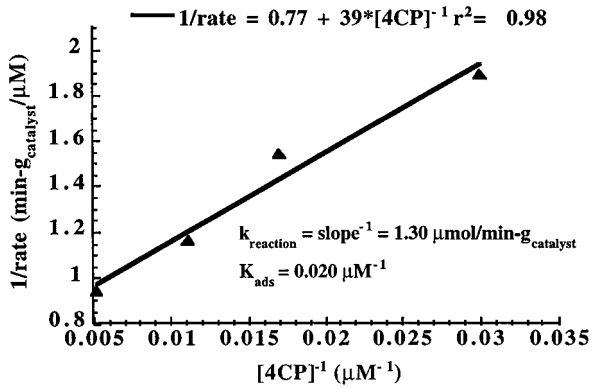

FIGURE 5. Langmuir–Hinshelwood reaction rate ($k_{reaction}$) and adsorption equilibrium (K_{ads}) constant determination for the slurry-phase photocatalytic oxidation of 4CP. Reciprocal reaction rate is plotted versus reciprocal concentration. Reaction conditions are given in the text.

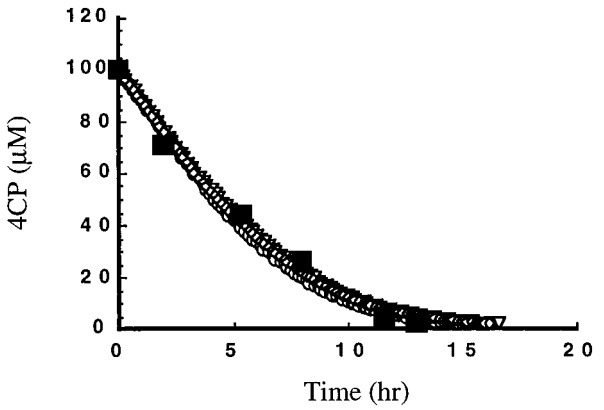

FIGURE 6. 4CP oxidation profile: (B) OFR experimental data; and model data for (E) $\phi_{global} = 0.031$, (S) $\phi_{global} = 0.037\,I'^{-0.3}_{abs}(z)$, (S) $\phi_{global} = 0.042 I'^{-0.5}_{abs}(z)$. $I_{input} = 0.31\,\mu E\,L^{-1}\,min^{-1}$ and $K_{ads} = 0.020\,\mu M^{-1}$. Reaction conditions are given in the text. $\hat{s} = 300\,\mu mol/g$, $\omega = 0.48$ g L^{-1} and $\hat{\omega} = 4.1\,\mu M$ TiO_2 particles.

TABLE 2. Best Model Fit Values for *A* and Calculated $(\phi_{global})_{avg}$ for Various Expressions for ϕ_{global} Having a 0, −0.3, and −0.5 Power Dependency on $I'_{abs}(z)$[a]

expression for $\phi_{global}(I'_{abs})$	I_{input}	A/ϕ_{avg} 4CP	PCP	DCA
AI_{abs}^{0}	0.3	0.031/0.031[b]	0.077/0.077[e]	0.25/0.25[b]
$AI_{abs}^{-0.3}$	0.3	0.037/0.042[b]	0.092/0.104[e]	0.31/0.35[b]
$AI_{abs}^{-0.5}$	0.3	0.042/0.055[b]	0.105/0.137[e]	0.35/0.46[b]
ϕ_{exp}	0.3	0.012	0.015	0.095
AI_{abs}^{0}	0.43	0.031/0.031[d]		
ϕ_{exp}	0.43	0.009		
AI_{abs}^{0}	0.47	0.024/0.024[c]		
ϕ_{exp}	0.47	0.008		

[a] Here, per fiber I_{input} equals the measured $I_{abs(bundle)}$/72 fibers, $\hat{s} = 300$ μmol/g, $\omega = 0.48$ g L^{-1}, and $\hat{\omega} = 4.1\,\mu M$ TiO_2 particles. [b] Measured $I_{abs(bundle)} = 22$,[b] 31,[c] 34,[d] and 20[e] $\mu E\,L^{-1}\,min^{-1}$.

$$(\phi_{global})_{avg} = L^{-1}\int_0^L \phi_{global}(I'_{abs}(z))\,dz \qquad (13)$$

The calculated average global quantum efficiencies are consistently higher than the experimentally determined relative quantum efficiencies but are typically within a factor of 5. Model $(\phi_{global})_{avg}$ of 0.031, 0.077, and 0.25 are calculated for case 1 as compared to 0.012, 0.015, and 0.095 relative quantum efficiencies for the 4CP, PCP, and DCA oxidations, respectively. The intensity-independent case gave the lowest global quantum efficiency values while the inverse square

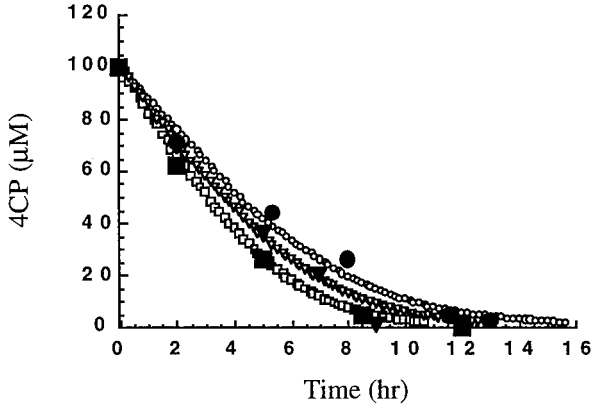

FIGURE 7. 4CP oxidation profiles: OFR experimental data for I_{input} equal to (J) 0.31, (B) 0.43, and (P) 0.47 μE L^{-1} min^{-1}; and model data for case 1: ϕ_{global} = (E) 0.031, (S) 0.031, (S) 0.024. I_{input} = 0.31 μE L^{-1} min^{-1} and K_{ads} = 0.020 μM^{-1}. Reaction conditions are given in the text. $\hat{s}$ = 300 μmol/g, ω = 0.48 g L^{-1}, and $\hat{\omega}$ = 4.1 μM TiO_2 particles.

root case gave values that were a factor of 2 higher. The model was also run for case 1 for three different input/absorbed light intensities of 0.31, 0.43, and 0.47 μE L^{-1} min^{-1} for 4CP (Table 2). The results are plotted in Figure 7. ϕ_{global} [= $(\phi_{global})_{avg}$] was calculated to be 0.031, 0.031, and 0.024, respectively.

Discussion

The above model characterizes mathematically the OFR system and identifies several important reactor/reaction parameters. Critical assumptions in development of the model are that (a) the reaction occurs on the surface of TiO_2, (b) the reaction rate is controlled by electron-transfer kinetics and is not controlled by adsorption kinetics or is not mass transport limited, (c) the photochemical reactions are symmetrical with respect to each coated fiber, and (d) the reaction is not limited by O_2 sorption or by competitive inhibition from reaction intermediates or other solution species. In addition, the estimated values for γ and $\hat{s}$ (i.e., 4.16×10^5 molecule/TiO_2 particle and 300 μmol of sites/g of catalyst, respectively) may have wider ranges and thus affect the quality of the agreement between the model calculations and the experimental observations.

It is widely accepted that heterogeneous photocatalytic reactions occur on or near the surface and can be represented by a Langmuir−Hinshelwood kinetic expression (*7*, *20*, *22*, *24*, *25*). Many studies involving slurry-phase reactors have reported no evidence of mass-transport limitations (*18*, *20*, *24*, *26*−*29*). In contrast, mass transport effects in fixed-bed photocatalytic reactor systems appear to be a function of the reactor design and reaction parameters such as distribution of the photocatalyst within the reaction volume, the radiation field with respect to the exposed photocatalyst membrane, pollutant concentration, and reaction solution flow rate (*19*, *27*, *29*−*32*). The close, concentric arrangement of fibers within the oxygen-saturated reaction solution of the OFR coupled with vigorous mixing and slow reaction rates (e.g., 0.3−2 μM min^{-1}) suggest that it is reasonable to assume the system is in equilibrium and that it is not mass-transport limited. In addition, it has been previously demonstrated that the TiO_2 coating is highly porous (e.g., porosity ≈ 0.9) and that mass transport within the coating and within the OFR reaction volume, in general, is not rate limiting (*1*, *2*). Sparging with oxygen ensures that the reaction solution is O_2 saturated. The assumption of no competitive inhibition by products or intermediates is made to simplify the model even though it has been shown that reaction intermediates can significantly affect the reaction rate of the parent compound (*19*, *26*). In addition, Cl^- and other inorganic anions have been found to compete effectively for surface sites and may play a significant role in the reaction rate of the chlorinated parent compound (*33*). A more elaborate model can be developed to incorporate these nonlinear competitive factors but will be assumed here to be constant and represented in the ϕ_{global} term.

The relationship between the observed reaction rate constant, the relative quantum efficiency, and the normalized absorbed light intensity is analogous to direct photolysis rate expressions of the form

$$-\frac{dC_R(t)}{dt} = \phi(\lambda) I_{input}(\lambda, t)(1 - e^{-2.303\epsilon l C_R(t)}) \qquad (14)$$

where λ is the wavelength-dependent photolysis quantum efficiency, ϵ is the substrate extinction coefficient, and l is the path length of radiation (*34*−*37*). In the case of a heterogeneous reaction, the light-absorbing reactant (i.e., the TiO_2 photocatalyst) is assumed to be a complete absorber of the radiation, and the third term in eq 14 becomes unity (*7*, *22*).

In our model, the absorbed photon flux is normalized by the photocatalyst particle concentration, $\hat{\omega}$, to account for the distribution of photon flux within the photocatalytic coating. In illuminated semiconductor photocatalysts, charge-carrier (e^-, h^+) recombination and interfacial charge transfer are second- and first-order processes, respectively. The charge-carrier density increases with an increase in the absorbed light intensity. As a result, at a higher relative absorbed light intensity, the rate of charge-carrier recombination is increased relative to interfacial charge transfer, and this leads to a lower quantum efficiency. This approach is consistent with previous findings regarding the relationship between measured relative quantum efficiencies and normalized absorbed light intensities (*1*). Based on the above assumptions, experimental and empirical determination of the various model parameters provides a basis for calibrating the model against experimental data.

The extent of the refractive losses of light out of a coated fiber was found to be a function of the interfacial contact area between the TiO_2 particles and the quartz fiber surface (i.e., the greater the contact area, the greater the refractive loss over a given length) (*2*). Parameters such as the coating porosity, particle size, and coating method affect the interfacial contact area. In our earlier work (*1*, *2*) with the OFR systems, we showed that the amount of light absorbed (I_{abs}) was clearly a function of the coating thickness; for example, at a coating slurry concentration of 13% by weight, 95% of the incoming light was absorbed by the TiO_2 coating. The above phenomenon is reflected in a higher α value for the higher TiO_2 wt % coating shown in Figure 3. An α value of 20 m^{-1} is used in the model that corresponds to a 13 wt % coating employed in the oxidations.

Similarly, an empirical relationship for the quantum efficiency dependence on the absorbed light intensity is derived from experimental data for the photocatalytic oxidation of 4CP (Figure 4). A fit of the data from the OFR yields $\beta \approx 0.3$. This value suggests operation in a low to moderate absorbed light intensity region (i.e., a value of β between 0 and 0.5). The spatially-averaged estimate of β is reasonable since the per fiber input light intensities, I_{input}, are on the order of 10^{-6} Einstein min^{-1} (approximately 1 sun). The *local* absorbed light intensities to which the photocatalyst coating is exposed, however, is a small fraction of I_{input}. Therefore, one would expect that the corresponding *local* quantum efficiency to be independent of $I'_{abs}(z)\,dz$, i.e., $\beta = 0$. The value for $I_{input} = 0.3\,\mu$E L^{-1} min^{-1} was estimated based on a typical measured absorbed light intensity for the bundle, $I_{abs(bundle)}$, divided by the number of fibers in the

bundle ((22 μE L^{-1} min^{-1})/72 fibers). This estimation assumes uniform distribution of the input beam into the bundled fibers. Based on this analysis, we conclude that an intensity-independent quantum efficiency expression is the most appropriate.

In a photocatalytic reaction system, the quantum efficiency is a measure of the efficiency of photon utilization with respect to the disappearance of the parent compound or appearance of a reaction product (eq 2). ϕ embodies many elements of the reaction scheme such as charge-pair generation/recombination, formation of radical intermediates such as $OH^{\bullet}$ and $O_2^{\bullet -}$, electron transfer, and H-atom abstraction, etc. (eq 3). However, only the normalized absorbed light intensity is used to weight the quantum efficiency term in the model. In this case, all other reaction parameters are assumed to be constant and are incorporated into the preexponential term, *A*.

For the intensity-independent case (case 1), *A* is equal to $(\phi_{global})_{avg}$ and is within a factor of 2.5, 5, and 2.5 of ϕ_{exp} for the 4CP, PCP, and DCA degradations, respectively. The higher model values indicate that the effect of competing intermediates on the reaction may not be constant and cannot be incorporated into *A* or may be due to inaccuracies in the estimation of some of the model parameters such as the K_{ads}, coating thickness, porosity, I_{input}, γ, $\hat{s}$, etc. When the model is run for 4CP at three different light intensities and compared to experimental data, $(\phi_{global})_{avg}$ is reasonably constant with values of 0.031, 0.031, and 0.024. A constant value is expected since all other reaction parameters have been held constant in the experimental system.

Although the system is assumed not to be mass-transport limited based on our previous calculations (*2*), a mass-transport limited condition could be incorporated into the model by introducing a combined reaction rate constant that is a function of a mass transfer and a reaction rate term (*18*) as follows:

$$k_{obs} = \left(\frac{1}{\text{mass transfer term}} + \frac{1}{\text{reaction rate term}}\right)^{-1} \quad (15)$$

The empirically-derived reaction rate and adsorption equilibrium constants for 4CP are consistent with values found in the literature, even though they were derived under vastly different reaction conditions. The corresponding values are $k_{4CP} = 1.5\ \mu mol/(min \cdot g_{catalyst})^{-1}$, $K_{ads} = 0.030\ \mu M^{-1}$ (0.5 g L^{-1}, pH 2, 48 W blacklight) (*38*); $k_{4CP} = 2.6$, $K_{ads} = 0.017$ (2 g L^{-1}, 125 W Hg lamp) (*10*); $k_{4CP} = 78.6$, $K_{ads} = 0.006$ (1 g L^{-1}, pH 3.5, 20 W blacklight) (*39*). Ollis et al. (*40*) report values of $k = 20\ \mu mol\ (min \cdot g_{catalyst})^{-1}$ and $K_{ads} = 0.022\ \mu M^{-1}$ for the slurry-phase photocatalytic oxidation of DCA using 0.1 wt % Fisher TiO_2 (95% anatase, 7 m g^{-1} surface area, 7 $\times$ 15 W blacklights, pH not given). The discrepancy between these values and those of the present study may be a result of different reactions conditions employed. No explicit reaction rates or absorption equilibrium constants were found in the literature for the photocatalytic oxidation of PCP.

A mathematical model of a fiber-optic bundled array reactor system is developed using Langmuir−Hinshelwood kinetics and compared to experimental data. A global quantum efficiency, ϕ_{global}, is defined and used as a model fitting parameter. It incorporates reaction parameters such as the absorbed light intensity, the intrinsic rate constant, and the effects of other adsorbed reactants and reaction intermediates. An empirical term to describe the radiation field within the coated fiber is derived experimentally and normalized by the coating photocatalyst particle concentration to account for the inverse relationship between the absorbed light intensity and the reaction quantum efficiency. ϕ_{global} was determined to be independent of the absorbed light intensity, and calculated values are consistent with the experimentally observed values.

Acknowledgments

We are grateful to ARPA, NSF (BES-9619885), and ONR (NAV 5 HFMN N000149J1901) for financial support and to Prof. George Gavalas, Janet Kesselman, and Tom Lloyd for their helpful discussions. We would also like to thank 3M and Degussa for their donations of the optical fiber samples and the P25 photocatalyst, respectively.

Literature Cited

(1) Peill, N. P.; Hoffmann, M. R. *J. Solar Energy Eng.* **1997**, *119*, 229−236.
(2) Peill, N. J.; Hoffmann, M. R. *Environ. Sci. Technol.* **1995**, *29*, 2974.
(3) Peill, N. J.; Hoffmann, M. R. *Environ. Sci. Technol.* **1996**, *30*, 2806−2812.
(4) Peill, N. J.; Bourne, L.; Hoffmann, M. R. *J. Photochem. Photobiol. A: Chem.* **1997**, *108*, 221−228.
(5) Ollis, D. F.; Pelizzetti, E.; Serpone, N. *Environ. Sci. Technol.* **1991**, *25*, 1522−1529.
(6) Okamoto, K.; Yamamato, Y.; Tanaka, H.; Tanaka, M.; Itaya, A. *Bull. Chem. Soc. Jpn.* **1985**, *58*, 2015.
(7) Kormann, C.; Bahnemann, D. W.; Hoffmann, M. R. *Environ. Sci. Technol.* **1991**, *25*, 494−500.
(8) D'Oliveira, J. C.; Al-Sayyed, G.; Pichat, P. *Environ. Sci. Technol.* **1990**, *24*, 990.
(9) Mills, G.; Hoffmann, M. R. *Environ. Sci. Technol.* **1993**, *27*, 1681−1689.
(10) Al-Sayyed, G.; D'Oliveira, J. C.; Pichat, P. *J. Photochem. Photobiol. A: Chem.* **1991**, *58*, 99−114.
(11) Albery, W. J.; Brown, G. T.; Darwent, J. R.; Saievariranizad, E. *J. Chem. Soc. Faraday Trans. 1* **1985**, *81*, 1999−2007.
(12) Ollis, D. F. *Photochemical Conversion and Storage of Solar Energy;* Pellizzetti, E., Schiavello, M., Eds.; Kluwer Academic Publishers: Dordrecht, The Netherlands, 1991; pp 593−622.
(13) Marinangeli, R. E.; Ollis, D. F.; Alfano, O. M.; Negro, A. C. *AIChE J.* **1982**, *28*, 945−955.
(14) Ollis, D. F.; Marinangeli, R. E. *AIChE J.* **1980**, *26*, 1000−1007.
(15) Ollis, D. F.; Marinangeli, R. E. *AIChE J.* **1977**, *23*, 415−425.
(16) Gapen, D. C. Photocatalytic Degradation of Chlorinated Hydrocarbons. M.S. Thesis, University of Wisconsin, 1991.
(17) Ollis, D. F.; Turchi, C. *Environ. Prog.* **1990**, *9*, 229−234.
(18) Ollis, D. F.; Pelizzetti, E.; Serpone, N. *Photocatalysis: Fundamentals and Applications: Heterogeneous Photocatalysis in the Environment: Application to Water Purfication*; Serpone, N., Pelizzetti, E., Eds.; Wiley & Sons: New York, 1989; pp 603−637
(19) Lu, M. C.; Roam, G. D.; Chen, J. N.; Huang, C. P. *J. Photochem. Photobiol. A: Chem.* **1993**, *76*, 103−110.
(20) Turchi, C. S.; Ollis, D. F. *J. Catal.* **1990**, *122*, 178.
(21) Cassano, A. E.; Martin, C. A.; Brandi, R. J.; Alfano, O. M. *Ind. Eng. Chem. Res.* **1995**, *34*, 2155−2201.
(22) Hoffmann, M. R.; Martin, S. T.; Choi, W.; Bahnemann, D. W. *Chem. Rev.* **1995**, *95*, 69−96.
(23) Vasudevan, D.; Stone, A. *Environ. Sci. Technol.* **1996**, *30*, 1604−1613.
(24) Pruden, A. L.; Ollis, D. F. *J. Catal.* **1983**, *82*, 404−417.
(25) Hsiao, C. Y.; Lee, C. L.; Ollis, D. F. *J. Catal.* **1983**, *82*, 418.
(26) Matthews, R. W. *J. Catal.* **1988**, *111*, 264−272.
(27) Turchi, C. S.; Ollis, D. F. *J. Phys. Chem.* **1988**, *92*, 6852−6853.
(28) Matthews, R. W. *J. Phys. Chem.* **1988**, *92*, 6853−6854.
(29) Sabate, J.; Anderson, M. A.; Kikkawa, H.; Edwards, M.; Hill, C. G. *J. Catal.* **1991**, *127*, 167−177.
(30) Aguado, M. A.; Anderson, M. A.; Hill, C. G. *J. Mol. Catal.* **1994**, *89*, 165−178.
(31) Matthews, R. W. *J. Phys. Chem.* **1987**, *91*, 3328.
(32) Sabate, J.; Anderson, M. A.; Aguado, M. A.; Gimenez, J.; Cerveramarch, S.; Hill, C. G. *J. Mol. Catal.* **1992**, *71*, 57−68.
(33) Abdullah, M.; Low, G. K. C.; Matthews, R. W. *J. Phys. Chem.* **1990**, *94*, 6820.
(34) Noyes, W. A.; Leighton, P. A. *The Photochemistry of Gases*; Dover Publications: New York, 1941.
(35) Calvert, J. G.; Pitts, J. N. *Photochemistry*, 1st ed.; John Wiley & Sons, Inc.: New York, 1966; p 899.

(36) Seinfeld, J. H. *Air Pollution: Physical and Chemical Fundamentals*; 1st ed.; McGraw-Hill: New York, 1975; p 523.
(37) Willberg, D. M.; Lang, P. S.; Hochemer, R. H.; Kratel, A.; Hoffmann, M. R. *Environ. Sci. Technol.* **1996**, *30*, 2526−2534.
(38) Mills, A.; Morris, S. *J. Photochem. Photobiol. A: Chem.* **1993**, *71*, 75−83.
(39) Matthews, R. W. *Water Res.* **1990**, *24*, 653−660.
(40) Ollis, D. F.; Hsiao, C. Y.; Budiman, L.; Lee, C. L. *J. Catal.* **1988**, *88*, 89−96.

Received for review October 11, 1996. Revised manuscript received October 24, 1997. Accepted November 3, 1997.

ES960874E